Integrated transcriptome analysis of the cellular mechanisms associated with Ha-ras-dependent malignant transformation of the human breast epithelial MCF7 cell line

Franck Gadal*, Christophe Bozic[1], Céline Pillot-Brochet[1], Sophie Malinge[1], Sarah Wagner[1], Aurélie Le Cam[1], Laurent Buffat[1], Michel Crepin and François Iris[2]

Unité Inserm U 553, Hôpital St Louis, 75010 Paris, France and Université Paris 13, France, [1]Valigen, Tour Neptune, 92086 Paris La Défense, France and [2]Ecole Centrale de Paris, Grande voie des vignes, 92295 Chatenay Malabry, France

ABSTRACT

To understand the cellular mechanisms of malignant transformation induced by constitutive activation of the ras oncogene (Ha-ras), we used a subtractive hybridization method (VGID^{TM}) together with an integrative analytical procedure based upon literature databases in the form of extensive interaction graphs. We found 166 over- and under-expressed genes which, in the human MCF7-ras breast epithelial cell line, are involved in the different aspects of tumoral transformation such as defined signaling pathways, cellular growth, protection against apoptosis, extracellular matrix and cytoskeleton remodeling. Integrative analysis led to the construction of a physiological model defining cross-talk and signaling pathway alterations which explicitly suggested mechanisms directly involved in tumor progression. The model further suggested points and means of intervention which could induce cell death in Ha-ras-transformed cells specifically. These hypotheses were directly tested *in vitro* and found to be largely correct, hence indicating that these new analytical and technological approaches allow the discovery of pathology-associated cellular mechanisms and physiologically defined targets leading to phenotype-specific pharmacological interventions.

INTRODUCTION

Over-expression of the ras family of oncogenes is associated with tumorigenicity, invasiveness and metastatic potential in a variety of human breast carcinomas (1). However, in contrast to organisms with fully sequenced and annotated genomes, DNA microarray technologies are of limited usefulness in identifying and measuring changes in mRNA levels originating from human genes, the expression of which are affected by Ha-ras constitutive activation. Here, a technological approach, free of a priori choices, was used in order to gather primary expression data, unbiased enough to allow successful integration with extensive published information.

To investigate the mechanisms whereby Ha-ras activation leads to tumorigenic transformation, we chose two human breast cell lines which only differ by constitutive activation of the Ha-ras oncogene. The MCF7 cell line, cloned from a pleural effusion of breast adenocarcinoma, is non-invasive and estrogen-growth-dependent, whereas the same MCF7 cells stably transfected with Ha-ras (MCF7-ras) are sensitive to, but not dependent upon, estrogens and can spontaneously form tumors after implantation in the nude mouse (2,3).

The patterns of differential expression associated with tumorigenic transformation were analyzed using the Valigen Gene IDentification (VGID™) process, a technology based on a modified subtractive hybridization method (Fig. 1). The sequences differentially expressed in a MCF7-ras cDNA library ('Tester') are subjected to competitive hybridization against an excess amount of MCF7 cDNA library ('Driver') followed by selective trapping of all 'Driver' material, including sequences held in common by both 'Tester' and 'Driver', as well as single stranded 'Tester' cDNA, thus avoiding the construction of normalized cDNA libraries. Several iterative rounds of subtraction and selective trappings result in an efficient and high enrichment of 'Tester' specific sequences. This technology does not require specific probes or primers to isolate differentially expressed mRNAs, thus allowing identification of isoforms and unknown transcripts without having to predetermine the sequences to be investigated.

Primary differential expression data and extensive published information were then integrated into a detailed and experimentally testable biological model describing the mechanisms presumably implemented by Ha-ras constitutive activation, together with the points on which defined pharmacological intervention would specifically abrogate the tumorigenic phenotype (Fig. 2).

*To whom correspondence should be addressed. Tel/Fax: +33 1 48 38 77 20; Email: fgadal@club-internet.fr
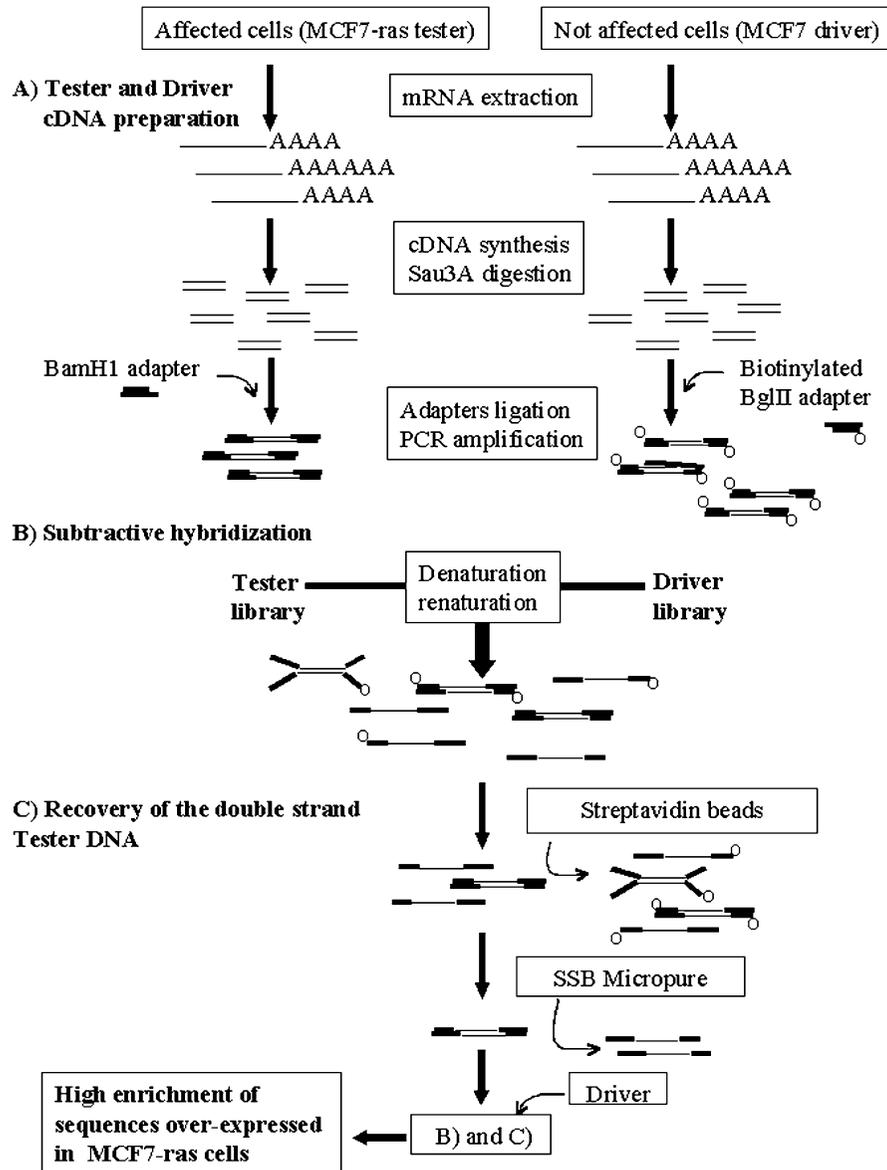
Figure 1. VGID™ subtractive DNA method. In order to obtain similar efficiency in the PCR amplification of each fragment, a four base cutting enzyme (Sau3A) was used to generate fragments of ~256 bp on average. The BamH1 and biotinylated BglII adapters were chosen to differentiate 'Tester' and 'Driver' populations. To enhance subtractive hybridization efficiency, all the Tester single stranded cDNA was removed using the SSB protein. Three consecutive rounds of differential trapping resulted in high enrichment of the over-expressed sequences from the Tester library.

This computational approach is based upon the weighted contextual indexation of the literature in terms of components and biological mechanisms associated with the systematic destruction of hypotheses arising from the injection of data into the indexed literature database (graph). The elements that result in a hypothesis being destroyed are in turn used to generate a new hypothesis which will then be submitted to the destructive process, and so on iteratively until a hypothesis which cannot be destroyed is obtained (Fig. 3). This does not mean that the hypothesis is correct; it merely means that it is supported by the existing publicly accessible information. Undestroyed hypotheses are then merged into 'meta-hypotheses' that are in turn subjected to the iterative destruction process. In this manner, one finally arrives at a theoretical

biological model entirely supported by published information which provides directly testable explanations for as yet poorly understood mechanisms. Should the biological data arising from these tests demonstrate that the model is largely incorrect, this new data can now be injected into the process to correct the model. Although requiring a considerable amount of work, this process is surprisingly fast (months as opposed to years).

The integrative procedure that we implemented consists of eight distinct steps (http://perso.club-internet.fr/fgadal). (i) Construction of an *in silico* relational graph encompassing all known functional interactions between genes, proteins and other small molecules recorded in the scientific literature pertaining to mammalian cellular and physiological
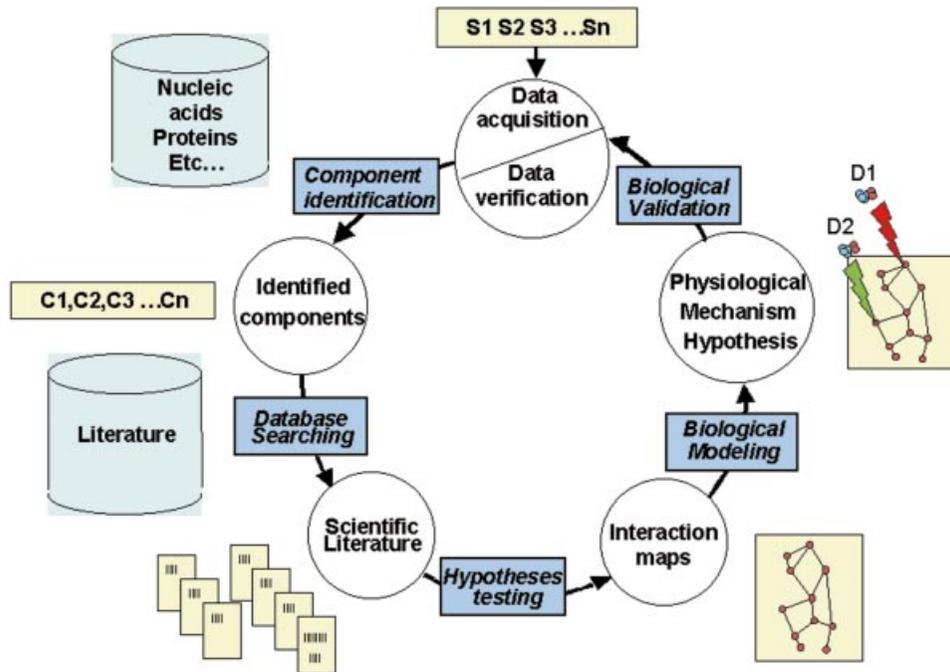
Figure 2. The integrative process. This diagram summarizes the algorithmic approach followed here for the integration of experimental data with published information. The circular shape given to this succession of steps is meant to underline both the iterative nature of this process as well as the fact that it does not have a uniquely defined starting point but can be implemented from any of its main steps.
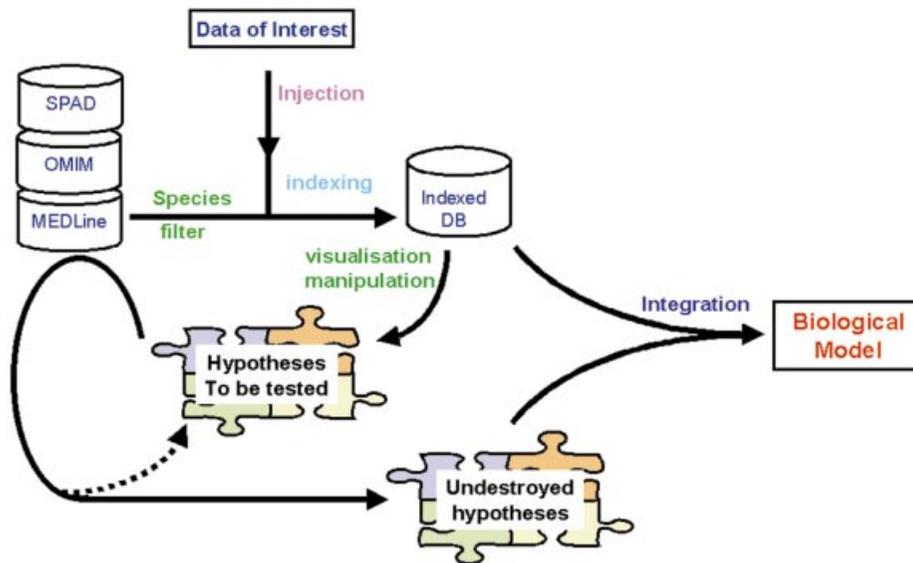
Figure 3. Overview of the computer-assisted model-building process. The model presented here resulted from the systematic destruction of 'working hypotheses' arising from the integration of experimental data with published information into an indexed database. The hypotheses that could not be destroyed were then merged into 'meta-hypotheses' that were in turn subjected to the destruction process. This lead to the production of a theoretical biological model, entirely supported by published information, that clearly indicated which aspects had to be experimentally verified, where, how and why.

mechanisms. (ii) Injection into the graph of the primary differential expression data set and extraction of the sub-graph containing the functional paths linking the data set components and identifying the biological elements associated with these paths. (iii) Integration of the resulting information into an initial model describing the pathways represented and the interactions governing pathway functions. (iv) Identification of the key genes and isoforms, absent from the primary data set, whose expression patterns govern cross-talk and functions within and between the pathways identified. (v) Construction of the appropriate DNA microarrays and direct verification of the expected expression patterns and expression

levels. (vi) Reiteration of steps (ii) and (iii). (vii) Identification of the physiological intervention targets and intervention modes which should specifically affect Ha-ras transformed cells. (viii) Direct experimental verification of the model's predictions.

Extensive data have been gathered over the years concerning the cellular mechanisms associated with tumors and tumor progression. However, this previous and widely dispersed work encompasses numerous genes, gene products as well as metabolic and physiological processes analyzed in a wide variety of contexts. While a substantial proportion of this work has been reduced to discrete pathways, most of the data remain functionally unconnected and expression data from higher eukaryotes have so far resisted integration into biologically coherent models. We report the first successful large scale integration of mammalian experimental gene expression data together with extensive physiological information extracted from public literature databases, and describe a theoretical biological model, validated *in vitro*, which, by exposing regulatory and cross-talk interactions associated with Ha-ras-dependent transformation, attempts to explain the mechanisms implemented in this complex pathological process.

MATERIALS AND METHODS

Cell culture

The epithelial cell line MCF7 was obtained from ATCC (Rockville, MD, USA) whereas MCF7-ras cell line, obtained from MCF7 cells transfected with the Ha-ras oncogene, was a generous gift from Dr Sommers (3). Both cell lines were characterized by DNA finger-printing. Cell lines were cultured in Dulbecco's modified Eagle's medium without phenol red, low glucose concentration (Gibco BRL) supplemented with 10% Fetal Calf Serum (FCS) (Gibco BRL), 50 µg/ml streptomycin (Gibco BRL), 50 IU/ml penicillin (Gibco BRL) and 0.3 mg/ml L-glutamine (Gibco BRL).

cDNA synthesis

Direct mRNA capture from lysed cell cultures was performed using Dynabeads® mRNA™ direct kit (Dynal) according to the manufacturer's protocol. First strand cDNA synthesis was carried out as follows: 6 µl aliquots of first strand synthesis mix [10 mM dNTP each (Promega), 0.1 M DTT and 5× first strand buffer (both from Life Technologies)], approximately 500 ng of Dynabeads®-bound denatured mRNA and 200 U Superscript II (Life Technologies) were separately pre-incubated to 37°C for 1 min in a water bath and then mixed. Following mixing, the components were incubated at 37°C for 1 h in a final volume of 30 µl. The first strand samples were then added to 170 µl aliquots of diluted second strand synthesis mix [10× *Escherichia coli* DNA ligase buffer (New England Biolabs), 900 mM KCl (Sigma), 20 mg/ml glycogen (Boehringer), 10 mM dNTP each, 10 U/µl *E.coli* DNA ligase (NEB), 2 U/µl Rnase H and 10 U/µl *E.coli* DNA polymerase I, all purchased from Promega] and incubated for 2 h at 16°C in a Perkin Elmer 9700 thermal cycler. The cDNA populations, still bound to Dynabeads, were then digested with *Sau3A* (4 U/µl New England Biolabs) for 2 h at 37°C, generating fragments of about 256 bp in statistical length, then the enzyme was inactivated for 20 min at 65°C. Adaptors were then ligated to the digested cDNAs (biotinylated adapters for the driver libraries) and PCRs were performed with adaptor specific primers on a Perkin Elmer 9700 thermal cycler, using 12 cycles of 95°C for 30 s, 55°C for 45 s, 72°C for 1 min followed by 72°C for 7 min. The PCR products were purified using a Qiaquick PCR purification kit (Qiagen) and utilized for VGID™ or micro-array experiments (see below). VGID™ and micro-array cDNA experiments were performed using RNA from independent cell cultures.

Adapters and oligonucleotides

Sequences of adapters (Cybergene) used in the VGID process were as follows: BamHI adapter, 5′CTT AGA ACG AGA CGG ATC CT3′ and 3′TT GAA TCT TGC TCT GCC TAG GAC TAGp5′, BglII-bio adapter, bio 5′CCA GCT AAC ACC TAG ATC TC3′ and 3′TT GGT CGA TTG TGG ATC TAG AGC TAGp5′. The cDNA fragments ligated to these adapters were amplified with the corresponding oligonucleotides (Cybergene): BamHI primer, 5′AA CTT AGA ACG AGA CGG ATC CTG ATC3′ and BglII-bio primer, bio 5′AA CCA GCT AAC ACC TAG ATC TCG ATC3′. The inserts were amplified with the primers pVG17 (–74), 5′GCA AGG CGA TTA AGT TGG GTA3′ and pVG17reverse (–88), 5′CTT CCG GCT CGT ATG TTG TGT3′.

VGID^TM gene identification technology (see patent no. 6 221 585)

VGID™ directly isolates over-expressed and under-expressed cDNA (Fig. 1) associated with the transition from one defined phenotypic state to another defined phenotypic state within a congenic system. For the first denaturation–renaturation step, 300 ng of BamHI-ligated-amplified Tester was mixed with 1200 ng BglII-bio-ligated-amplified Driver. The mixture was ethanol precipitated, and resuspended in 4 µl HEPES and EDTA. The solution was overlaid with 20 µl mineral oil, denatured for 5 min at 98°C and chilled on ice. The salt concentration was adjusted to 0.5 M with 1 µl 2.5 M NaCl. After a new denaturation of 5 min at 98°C, the sample was allowed to anneal for 20 h at 65°C. Following hybridization, the oil was removed, the sample volume was brought to 100 µl with 100 mM NaCl, 10 mM Tris–HCl pH 8 and mixed with 210 µl of streptavidin magnetic beads (10 mg/ml, Boehringer-Mannheim) to recover the tester single- and double-stranded cDNA. After 20 min of incubation at room temperature, the supernatant was recovered as described by the manufacturer. This step was repeated once to remove all biotinylated cDNA. Then, to recover the tester double strand DNA, the supernatant, which contained unbiotinylated cDNA, was incubated with 1.5 µg of Single Strand Binding Protein (SSB, Promega) for 30 min at room temperature. The sample was loaded onto a Millipore Micropure EZ membrane (which retained the proteins) and centrifuged for 1 min at 20 800 *g* at room temperature. The flow through was combined with 1200 ng of Driver and the next round of hybridization was set up as described above. A total of three rounds of hybridization were performed. The cDNA recovered after the third round was amplified by PCR as described above with 25 cycles using the BamHI primer. The sequences under- or over-expressed were cloned into a modified pUC19 vector (Gibco BRL).

Cloning

The vector used for the cloning step was a derivative of the pUC19 vector where the 5′AATTCGGATCCA3′ pVG17 linker sequence replaced the pUC 19 polylinker EcoRI–HindIII. In order to avoid the cloning of chimeric structures, a 3:1 vector/insert DNA ratio was used. Fifty nanograms of vector were ligated to the cDNA recovered and amplified after subtraction, using one unit of ligase (Boehringer) in a final volume of 10 µl overnight at 16°C. The ligation reaction product was purified by the Geneclean procedure (BIO 101) according to the manufacturer's recommendation. Two microliters of purified ligation reaction were used to transform 50 µl of MAX Efficiency DH10B cells (Gibco BRL). Transformation was performed by electroporation at 1800 V using the EC100 Electroporator (E-C Apparatus Corporation). Immediately after electroporation, 500 µl of SOC Medium was added. The cells were shaken at 300 r.p.m. for 1 h at 37°C and an aliquot was spread on an LB plate containing 100 µg/ml ampicillin.

Sequencing

Isolated colonies were picked in 150 µl LB with 100 µg/ml ampicillin in order to make glycerol stocks. Four microliters of this solution were cycle-sequenced in a Perkin-Elmer thermal cycler with the AmpliTaq Gold DNA polymerase kit (Perkin Elmer) using 10 pmol of pVG17(–74) and pVG17rev(–88) primers in a final volume of 50 µl. A pre-PCR step at 95°C for 13 min allows the activation of the polymerase and bacterial lysis. Each of the 40 PCR cycles included three segments: 95°C for 30 s, 54°C for 1 min, 72°C for 2 min 30 s. The PCR products were sequenced without purification using the BigDye Terminator Cycle Sequencing kit and ABI Prism 3700 automatic DNA sequencer (Perkin Elmer Applied Biosystem). DNA sequencing of clones was performed to saturation (until identification of new genes fell to zero in spite of increasing numbers of clones sequenced).

Sequence analysis

The clone sequences were analyzed using in-house programs that were written in Perl. After removing the vector sequence, the repeats were masked and the masked sequences were compared to public databases using the blastn and blastx programs. Significance of the similarities were checked both at the nucleic acid and protein levels. Sequences were considered identified when matching a known homolog with a level of identity greater than 98% at the DNA level. Significant similarities at the protein level were considered whenever the sequence matched a protein sequence with a level of identity at least equal to 40%. The sequence data were then clustered using Fasta software.

Gene-specific microarray sequences

We used primer3 (http//www.genome.wi.mit.edu/cgi-bin/primer/primer3.cgi) to design primers to amplify specific genes and generated amplicons of 280–320 bp in length. 5′AGCGATGGCGAGATCAGTAT3′ and 5′GGCGACATG-TAGGACCTTGT3′ for MKK1, 5′GGAGCTCATGGACAC-ATCCT3′ and 5′TTCAGCTCTGGGTTGATCCT3′ for MKK3, 5′GGACCTGATGGAGACTGACC3′ and 5′ATAG-CCCTTGGAGTTCAGCA3′ for Erk1, 5′CAACCATCGA-GCAAATGAAA3′ and 5′GACTTGGTGTAGCCCTT-GGA3′ for Erk2, 5′GGTGATCCTGGTGAAGGAGA3′ and 5′AGTCCAGGGCTGACACAATC3′ for PKB1, 5GGCTC-CTTCATTGGGTACAA3′ and 5′AGTCGTGGAGGAGT-CACTGG3′ for PKB2, 5′AGAAGTGCTGGGTCCA-GAGA3′ and 5′GGGACCTTTGTTGATTGCAT3′ for MAPKAPK-2, 5′GACCAGCACAAGCTGTACCA3′ and 5′CCCACTGAGAAATTCCGTGT3′ for CaMKII beta, 5′CTAGCAAATCCAAGGGAGCA3′ and 5′GAGTCACCG-TGTCCCATTCT3′ for CaMKII delta, 5′ACGTCATCAT-CCACAAGCTG3′ and 5′AGTCAAGCCGTTCTTCTCCA3′ for ITPKI, 5′CATTTCAAGGGAGGAGGTGA3′ and 5′TTG-ACAATCTGGTCCTGCTG3′ for p85 IP3K, 5′GTGACGA-TGTGGTCGTGTTC3′ and 5′CTTCATCTCCACCTCCG-TGT3′ for IP3R3, 5′AGTACCTGGCCCCTGAGATT3′ and 5′CAGTTGTGGCAAACCACTTG3′ for PKA ca alpha, 5′GGTGCTGTCCAAAAAGAAGC3′ and 5′GGCCTGGTC-TTCAGAGAGTG3′ for CaMKK beta, 5′AGGGGGAAA-GATTACCTGGA3′ and 5′TCAAAGAAGGGATGGGT-GAG3′ for P38 delta, 5′TCCGAGGAGAAATTGAGGAA3′ and 5′TATCCGGCAAGACAGACCTT3′ for DKK1, 5′CAT-CGTGGGCTACAAGGACT3′ and 5′ACACCTTCTTTGCC-CATCAG3′ for Profilin, 5′CCTACCAGAGGGGATT-GTGA3′ and 5′GGGGTGCAGGACACATAACT3′ for ADAM15, 5′AGAGTTGCTCCCAAAAGGGT3′ and 5′ACCCTTTTGGGAGCAACTCT3′ for ADAM17, 5′GGG-TTTAATGTGGTGGATGC3′ and 5′CGCTCCAGTCTTCA-GTAGGG3′ for 67LR, 5′CAAGATCACCATCACCAACG3′ and 5′ATGGGGTTACACACCTGCTC3′ for HSP70 (see Table 2 for the corresponding accession numbers). MCF7-ras cDNA (1.5 ng) was used to perform the PCRs (final volume 50 µl) as follows: one cycle of 95°C for 13 min, 40 cycles of 95°C for 30 s, 55°C for 45 s, 72°C for 1 min followed by 72°C for 7 min. Using the pGEM®-T Easy Vector Systems kit (Promega), each PCR product was cloned in pGEMT vector, and transformed in JM109 cells (Promega).

Microarray construction

All the clones obtained from the subtraction process and the above gene-specific sequences were studied using microarray technology. Each clone was PCR amplified in a final volume of 100 µl using 20 pmol of each primer pVG17 (–74) and pVG17rev (–88), 10 nmol dNTPs and 1.5 U of *DyNazyme EXT*. After 13 min of enzyme activation at 95°C, 40 cycles were carried out (95°C for 30 s, 56°C for 1 min, 72°C for 1 min 30 s) with a final incubation time of 7 min at 72°C. The PCR products were purified with a Multiscreen PCR Kit (Millipore) according to the manufacturer's instructions and concentrated by Speedvac. The PCR products, resuspended in $3\times$ SSC and 11 yeast genes used as internal controls, were spotted in triplicate onto GAPS Amino Silane Coated Slides (Corning) with the GMS 417 arrayer (Genetic MicroSystem). The slides were UV cross-linked at 300 mJ, prehybridized in a 50% formamide, 0.1% SDS, 1% BSA, $5\times$ SSC buffer at 42°C for 1 h, then washed first in water, then in 95% ethanol and finally vacuum dried.

Microarray hybridization, scanning and data acquisition

500 ng of MCF7 and MCF7-ras cDNA, obtained as described above, were labeled by random priming with incorporation of Cyanine5-dUTP for the 'Tester' DNA and Cyanine3-dUTP

for the 'Driver' samples, respectively. After labeling, 'Tester' and 'Driver' cDNA samples were mixed, concentrated by evaporation under vacuum and resuspended in hybridization buffer (same as prehybridization buffer above, with Denhardt's solution replacing BSA). The two-labeled cDNA mix (MCF7 mixed with MCF7-ras) was then applied to the arrayed slides and hybridization was performed overnight at 42°C. The slides were then washed (5 min in $1\times$ SSC, 0.1% SDS, 3 min in $1\times$ SSC, 3 min in $0.1\times$ SSC, water, 95% ethanol dried) and scanned (GenePix 4000A from AXON). Accurate differential measurements (final fluorescence ratios) were obtained by taking the average of nine independent assays where each sequence was arrayed in triplicate. Visualization, quantification and gene expression analysis were performed using the GENEPIX 3.0 software. The data were normalized using a self-normalization method. Paired-slides normalization was carried out through dye-swap experiments: two hybridizations for two cDNA samples, with dye assignment reversed in the second hybridization. This procedure is detailed in the web article by Yang *et al.* (2000) (Normalization for cDNA Microarray Data; http://oz.Berkeley.EDU/users/terry/zarray/Html/normspie.html).

Testing of points and modes of intervention suggested by the model

The MCF7 and MCF7-ras cells were seeded in 24-well plates at a concentration of 10^4 cells/well in triplicate. During exponential cell growth phase (48 h after seeding), the growth medium was removed and replaced by 1 ml of fresh medium supplemented with A23187 Ca^{2+} ionophore (A23187)-DMSO stock solution (Sigma) diluted to various concentrations in water, or with dibutyryl-cAMP (db-cAMP) stock solution (Sigma) diluted to various concentrations in water, or with an association of A23187-DMSO stock solution diluted to 100 nM and db-cAMP diluted to various concentrations in water. After 48 h incubation, the cells were harvested with a trypsin solution and cell viability was estimated by Trypan Blue exclusion assay.

Apoptotic nuclei observations

Morphological changes characteristic of programmed cell death, including chromatin condensation and nuclear fragmentation, were visualized by 4′-6-diamino-2-phenylindole (DAPI) staining. Cells cultured on Lab-Tek chamber slides (Nunc Inc., Naperville, IL, USA) were treated with A23187 and/or db-cAMP as indicated. Adherent MCF7 and MCF7-ras cells were stained with the DNA-specific fluorochrome 4′-6-diamino-2-phenylindole (Boehringer-Mannheim Biochemical) in a 1 μg/ml methanol solution. Cell counts were performed within 20 min of staining on a Zeiss Axiophot epifluorescence microscope. Fragmented or condensed nuclei were scored as apoptotic. Intact or mitotic nuclei were scored as normal.

RESULTS

### Under- and over-expressed sequences in MCF7-ras as compared to MCF7 cells

As described in Materials and Methods, the sequences differentially expressed in a MCF7-ras-cDNA library

('Tester') were subjected to competitive hybridization against an excess amount of MCF7-cDNA library ('Driver') followed by the selective trapping of all 'Driver' material, including sequences held in common by both 'Tester' and 'Driver' and single-stranded cDNA (Fig. 1). For identification of the transcripts under-expressed in MCF7-ras, the process was repeated, using the MCF7-cDNA library as 'Tester'. All competitive hybridizations were performed using a ratio of 'Tester':'Driver' of 1:4 which allows an optimal recovery of sequences differentially expressed (data not shown). Three iterative rounds of subtraction and selective trapping resulted in high enrichment and efficient isolation of 'Tester' specific sequences that were then visualized by agarose gel electrophoresis, as shown in Figure 4. Gel migration analyses (1.5% agarose) were performed at each step of the process. Lanes 1 and 1′ correspond, respectively, to the MCF7 and MCF7-ras cDNA samples before differential trapping of sequences found to be over- and under-represented in the MCF7-ras library (Fig. 4, lanes 2 and 3, respectively). These results indicated that the two cDNA populations seem to be 'equivalent' with cDNAs ranging from 100 to 1500 pb in the two cases. Subtractive hybridizations resulted in the identification of 13 different major cDNA bands corresponding to cDNAs over-expressed in MCF7-ras (lane 2). Similar observations were made for the under-expressed MCF7-ras sequences: eight major bands (lane 3) correspond to over-expressed MCF7 sequences. Thus, differences in the electrophoresis profiles and in the number and length of the major bands (Fig. 4, lanes 2 and 3) are specific to the Ha-ras phenotype. In addition, cDNA sizes remained identical before and after *SAU3A*-adapter-amplification, suggesting that cDNA complexity was preserved (data not shown).

Overall, the VGID™ subtractive hybridization process yielded 740 cDNA inserts which were sequenced and cleaned using computer algorithms based in part on the recognition of the specific adaptors ligated to the cDNAs before cloning, thus eliminating empty vectors, and the quality of sequencing data was ascertained by bio-informatics analyses (PHRED software). Sequence analysis revealed that the VGID™ data set contained 166 cDNA sequences found to be differentially expressed in MCF7-ras versus MCF7 cells and that 28% of the total sequences were present more than twice while 63% were present at least twice. Of these, 106 corresponded to known transcripts encoding known functions, 41 to known transcripts/ESTs encoding unknown functions and 19 to new transcripts. Practically all the genes identified (over 95%) are known to have class II or class III expression levels (from 100 to less than 20 mRNA molecules/cell) (4) and most (over 80%) of these genes are known to be cancer-associated and/or epithelium-associated.

VGID™ process suggested activation of pathways dependent on the Ha-ras oncogene activation

Injection of the data set consisting of the 106 known transcripts into a relational graph of the entire 'PubMed' database (http://perso.club-internet.fr/fgadal), filtered by functional key words (such as activate, bind, inhibit, etc.) for exclusive retention of mammalian data (step i described in the Introduction), led to the extraction of a sub-graph depicting all known interactions, directly as well as indirectly, involving the injected elements (step ii). Of these 106 known transcripts
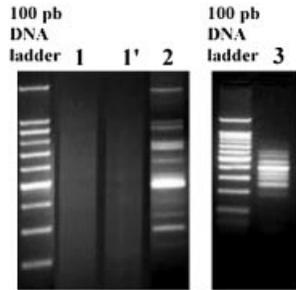
Figure 4. Gel migrations from VGID™ subtractive hybridizations. Gel migration analyses (1.5% agarose) were performed at each step of the process. Lane 1 and 1′ correspond, respectively, to the MCF7 and MCF7-ras cDNA samples before differential trapping of sequences over-represented in the MCF7-ras library (lane 2). For identification of the transcripts under-expressed in MCF7-ras, the process was repeated, using the MCF7 cDNA library as 'Tester'. Thus, lane 3 represents sequences under-represented in the MCF7-ras cDNA library after differential trapping.

studied in depth, 68 were integrated into defined cellular mechanisms (http://perso.club-internet.fr/fgadal). The other 38 known transcripts corresponded to gene functions that could not be so integrated but yielded important clues concerning cellular perturbations. Integrative analysis of the published information relative to the data set (step iii) indicated alterations in four different broad cellular mechanisms directly implicated in the Ha-ras transformation process (Table 1) which will be expanded in the Discussion. (i) Cytoskeleton assembly, with the under-expression of the actin-related complex 3 (Arp3), 27 kDa heat shock protein (Hsp27) and profilin, together with thymosin β4 and Leucocyte common Antigen Related protein (LAR) over-expression. (ii) Extra Cellular Matrix (ECM) dynamics, with the over-expression of ADAM 15 and 17, LAR, 67 Laminin Receptor (67LR), together with UDP-*N*-acetylglucosamine alpha1, 3-D-mannoside-beta1, 4-*N*-acetyl-glucosaminyltransferase (Gnt-IV), Fibulin-1 and Colligin/Hsp47 under-expression. (iii) Apoptosis regulation, with the over-expression of Hsp70 and 14.3.3.ε together with Bax-α and MA-3 under-expression. (iv) Growth cell stimulation, with activation of pathways dependent upon the p38 kinase (over-expression of rack-1, p38 delta and under-expression of Hsp27), Wnt (over-expression of Dickkopf-1 (DKK-1) and LAR) and inositol transduction signal [over-expression of the Calcium-calmodulin dependent protein kinase kinase β (CaMKKβ) and under-expression of profilin].

Validation and confirmation of the Ha-ras activated biological pathways by microarray analyses

Further integration of the functional information relative to these mechanisms led to the identification of specific regulatory and cross-talk alterations in detailed pathways governed by Extracellular signal-Regulated protein Kinase 1 (Erk1), but not Erk2, β-catenin/Wnt, Protein Kinase Cδ (PKCδ)/Mitogen Activated protein Kinase Kinase 3 (MKK3)-p38δ, Serine/threonine Protein Kinase B 1/2 (PKB1/2)/IκB and Phospholipase Cε (PLCε)/Inositol triphosphate Kinase subunit 85 (p85-IP3K), the cumulative effects of which would be the acquisition of a tumorigenic phenotype. However, this analysis clearly indicated that differential regulation of genes

playing key regulatory roles in these pathways, as well as in collateral mechanisms, would be necessary to achieve the suggested alterations (step iv). Thus, 13 pathway-specific genes, absent from the VGID™ data set, were selected for microarray expression analysis (Table 2, Fig. 5). Eight genes belonging to the previously ascertained VGID™ dataset were included as controls. Microarray analysis (step v) revealed that, as expected from the initial model, Ha-ras constitutive activation induces moderate to high over-expression of 10 of the selected genes. PKB1/2, Inositol triphosphate Kinase I (ITPKI), Inositol triphosphate Receptor 3 (IP3R3), p85-IP3K and Mitogen-Activated Protein Kinase-Activated Protein Kinase-2 (MAPKAPK-2), were found to be up-regulated more than 2-fold, while MKK3, Erk1, Calcium/calmodulin dependent Kinase IIδ (CaMK IIδ) and Protein Kinase A catabolic α subunit (PKAcaα), were up-regulated between 1- and 2-fold. Also as expected, MKK1 and Erk2 were down-regulated between 1- and 2-fold while CaMK IIβ was not differentially expressed (Table 2). Injection of this data into the integrative process (step vi) led to the construction of a detailed biological model suggesting the possible mechanisms of Ha-ras-mediated tumoral transformation (Fig. 6A). This model suggests that calcium-dependent pathways play a key role in the Ha-ras-mediated tumoral transformation. The deregulation of genes such as profilin, p85 IP3 kinase, IP3 R3, ITPK1 involved in calcium influx, gave indications of increased calcium mobilization within the cell. These increases in free calcium could lead to the activation of the CaMKKs and PKC/p38 delta signaling pathways and the down-regulation of the apoptotic pathway through the activation of PKB 1/2. Here, PKA/cAMP signaling activity controls CaMKKs-dependent pathways and the negative feedback mechanisms (Fig. 6A).

Specific death of the MCF7-ras cells using points and modes of intervention suggested by the integrative model

Analysis of the Ha-ras model (Fig. 6A) for identification of the points and modes of intervention most likely to affect the tumoral phenotype (step vii) indicated the calcium-dependent pathways and the PKA-mediated mechanisms as prime intervention targets. According to this analysis, receptor-independent calcium influx, mediated by low to moderate doses of A23187, in the presence of db-cAMP, known to maintain PKA activity while preventing a decrease in endogenous cAMP levels, should be sufficient to induce MCF7-ras-specific cell death by exacerbating the deregulation of the calcium-dependent pathways and negative feedback mechanisms. This hypothesis was directly tested *in vitro* by treatments of MCF7 and MCF7-ras cell cultures using the above drugs singly and in combination. Up to a concentration of 100 nM (Fig. 7A), A23187 had slight negative effects on MCF7 (~90% of viability) and more marked, but still moderate, effects upon MCF7-ras (65% of viability with 100 nM of A23187). Beyond this concentration, the negative effects became equally large on both cell lines. db-cAMP had no significant differential effects on either cell line up to a concentration of 100 μM (Fig. 7B). Beyond this concentration and up to 500 μM, db-cAMP had differential effects upon MCF7 cell survival, qualitatively similar to those of A23187 at a concentration of 100 nM (~80% of viability for MCF7 cells at a db-cAMP concentration equal to 500 μM) while
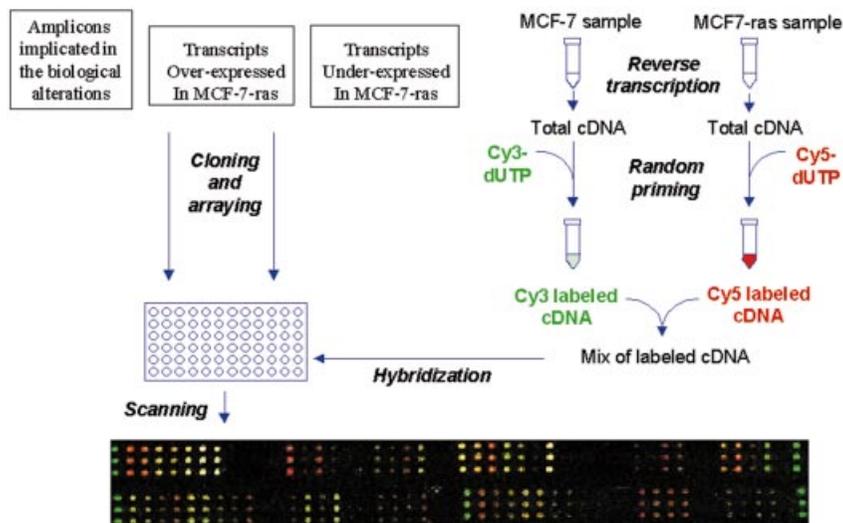
Figure 5. Differentially expressed status of VGID™-isolated transcripts validated by microarray quantitative expression analyses. MCF7 and MCF7-ras total cDNA samples were labeled by random priming with incorporation of Cy^5-dUTP for the 'Tester' cDNA (MCF7-ras) and Cy^3-dUTP for the 'Driver' cDNA (MCF7). The two labeled cDNAs were then mixed and hybridized to slides arrayed with VGID™-isolated transcripts as well as with amplicons corresponding to genes implicated in the biological alterations suggested by the VGID™ dataset (Table 2). In the scan window, green colour corresponds to cyanine 3 fluorescence and red colour to that of cyanine 5. For any given spot, orange to yellow relative intensities correlate with, respectively, over-expression or under-expression of the corresponding gene in MCF7-ras while pure red or green correspond to near unilateral expression of the corresponding genes in MCF7-ras or MCF7 cells, respectively.

quantitatively more marked on MCF7-ras (43% of viability at a db-cAMP concentration equal to 500 µM). When the two drugs were concurrently present (Fig. 7C), differential effects, stronger than those previously observed with A23187 alone, became apparent at concentrations where db-cAMP had previously been without significant effects. The best differential response was obtained with a treatment consisting of 100 nM A23187 + 400 µM db-cAMP. Here, at least 80% of the MCF7 cells remained viable, a survival level closely similar to that previously observed with either DMSO control medium (data not shown), or 100 nM A23187 alone or 400 µM db-cAMP alone. In contrast, only 36% of the MCF7-ras cells remained alive after treatment, as compared to 65% surviving cells at a A23187 concentration equal to 100 nM and 71% surviving cells at a db-cAMP concentration equal to 400 µM. Cell death was evaluated using the documented observation that dying or dead cells accumulate Trypan Blue. Since the treatment leading to cell death did not include cytotoxic compounds, cell death was likely to be largely due to apoptosis. This was confirmed by fluorescence microscopy observation of treated cells after DAPI staining of nuclei. Chromatin condensation and DNA fragmentation, indicated by arrows in Figure 8 and practically absent in the untreated cell samples (Fig. 8C), were observed mainly in MCF7-ras treated with the two drugs (Fig. 8B) as compared to MCF7 (Fig. 8A). The combination of drugs exhibited clear deleterious cumulative effects upon the Ha-ras transformed cell line while leaving the non-transformed parental cell-line essentially unaffected, hence substantiating the MCF7-ras-specific effects indicated by the model.

DISCUSSION

The VGID process allows the isolation of cDNA clones representing genes differentially expressed within two RNA populations while microarray analysis allowed us to independently test the expression patterns of selected genes. In the present study, the originality of our analytical approach resides in the combination of subtractive hybridization, cDNA microarray and data integration. We combined subtractive hybridization and cDNA microarray to identify new genes associated with the expression of the Ha-ras oncogene in the MCF7 cell-line (for entire data, see web page at http://perso.club-internet.fr/fgadal). This technology is rapid (hybridization takes place within 20 h), sensitive (detection of rare cDNA species with low differential expression level) and economical (small amounts of mRNA are needed for cDNA library synthesis). Moreover, since the capture of biotinylated cDNA and single-stranded cDNA is very effective, the construction of normalized cDNA libraries is avoided and a significantly greater number of genes are correctly identified as compared to SSH. For all these reasons, VGID is more effective than SSH in isolating and identifying differentially expressed sequences. In this context, microarrays only allow assessment of the expression patterns of selected genes. In other words, one must first decide which genes to investigate prior to performing the analysis. In the present case, we decided not to introduce an analytical bias through the a priori selection of genes to be investigated. We thought it more appropriate to let the cells 'tell us' what to investigate. This precluded the use of probes and therefore the utilization of microarrays. We therefore had to devise an efficient and effective means to access unidentified differentially expressed sequences, hence the use of VGID followed by microarray-based verification. We then carried out computer-assisted data integration to achieve an understanding of the physiological mechanisms potentially affected by the genes confirmed to be differentially expressed. Microarray analysis confirmed both the patterns and levels of differential expression of the majority (90% of the entire data) of the genes identified as

Table 1. Cellular mechanisms directly implicated in the Ha-ras transformation process

| Broad cellular functions	Genes	Accession number	Blast homology	VGID™ status	Micro-array level expression (x-fold under- or over-expressed)
PKC activation and Ca²⁺ store mobilization	DAGK ζ	NM_003646	2.00E-60	↑	↑ 1.43 ± 0.29
	Reticulocalbin	NM_002901	1.00E-168	↑	↑ 7.24 ± 0.29
	Rack 1	AF146043	2.00E-100	↑	↑ 1.55 ± 0.10
	CaMKK β	AF140507	3.00E-56	↑	↑ 1.80 ± 0.17
	TCP 1θ	Z37164	1.00E-152	↑	↑ 2.18 ± 0.23
	Annexin VI	NM_001155	1.00E-105	↑	↑ 10.51 ± 1.35
Induction of PKC pathways	p38δ kinase	AF092535	1.00E-128	↑	↑ 3.29 ± 0.76
	FKBP52	M88279	1.00E-130	↑	↑ 1.37 ± 0.14
	DKK 1	AF177394	0.00E+00	↓	↓ 8.33 ± 0.03
Cytoskeleton remodeling	STE 5	L01620	8.00E-82	↑	↑ 1.12 ± 0.04
	LAR	Y00815	1.00E-117	↑	↑ 1.34 ± 0.08
	NHE3RF	AF036241	1.00E-64	↑	↑ 1.59 ± 0.13
	L-Plastin	NM_002298	2.00E-88	↑	↑ 1.60 ± 0.12
	Thymosin β4	M17733	4.00E-83	↑	↑ 1.20 ± 0.12
	ARP 3	NM_005721	1.00E-139	↓	↓ 1.25 ± 0.1
	Profilin 1	NM_005022	1.00E-78	↓	↓ 1.43 ± 0.2
	HSP 27	NM_001540	7.00E-91	↓	↓ 1.30 ± 0.14
Cell surface proteins	ADAM 17	NM_003183	1.00E-118	↑	↑ 2.03 ± 0.08
	ADAM 15	NM_003815	8.00E-79	↑	↑ 2.30 ± 0.11
	67 LR	NM_002295	1.00E-141	↑	↑ 2.03 ± 0.10
	PTK 7	NM_002227	0.00E+00	↑	ND
	TGFβ-masking protein	AA134236	1.00E-129	↓	ND
	Agrin/follistatin	AF016903	1.00E-77	↓	↓ 1.33 ± 0.12
	Podocalixin	NM_005397	1.00E-178	↓	ND
	Fibulin-1	NM_006487	4.00E-79	↓	↓ 1.51 ± 0.07
	Caveolin 1	AF125348	0.00E+00	↓	↓ 5.55 ± 0.18
	CD24	NM_013230	4.00E-80	↓	↓ 1.25 ± 0.10
	Gnt IV	AB000616	1.00E-158	↓	↓ 1.43 ± 0.14
	APR-3	NM_016085	1.00E-90	↓	↓ 1.37 ± 0.07
	Hsp47/colligin	X61598	1.00E-176	↑	↑ 1.33 ± 0.14
Survival mechanisms	HSP 70	M59828	7.00E-56	↑	↑ 1.68 ± 0.28
	14.3.3.ε	U43430	3.00E-100	↑	↑ 1.44 ± 0.09
	Bax-α	L22473	1.00E-149	↓	1 ± 0.09
	MA-3	AA585361	1.00E-144	↓	↓ 1.82 ± 0.05

Out of the 106 functionally characterized transcripts contained in the VGID™ data set, the 34 transcripts listed in the table played an important part in the integrative process, which led to the construction of a primary model of Ha-ras-dependent malignant transformation. The levels of expression indicate over-expression (upward pointing arrows) and under-expression (downward pointing arrows) in MCF7-ras as compared to MCF7. These expression patterns were qualitatively verified *a posteriori* by microarray expression analyses (Fig. 5). ND corresponds to a detection failure.

differentially expressed through the utilization of VGID. However, Yang *et al.* (5a), have suggested that quantitative information obtained using small cDNA inserts as well as clones arising from less abundant mRNA species could be unreliable due to their propensity to generate weak signals falling within the 'noise' of microarray hybridization signals. This may explain the few cases of non-concordance observed between VGID outputs and microarray analyses. Assuming that the number of isolates corresponding to a given transcript provides a rough representation of its relative abundance, our results indicate that the transcripts corresponding to the clones that failed the microarray cross-validation tests could well belong to low abundance classes since each of these transcripts was represented by only one isolated clone (data not shown). However, several genes found to be significantly differentially expressed using microarrays do not feature in the VGID data sets. This could be explained by limitations at several steps of our procedure such as cloning, sequencing to a saturating proportion of the clones (we stopped sequencing when the probability of finding new genes tended to zero) and the fact that some transcripts have no or only one *SAU3A* site

(corresponding to 10% of the human genome) thereby escaping adapter-dependent amplification. Despite its limitations, our approach allowed us to isolate and screen a large number of transcripts suggestive of physiological mechanisms associated with the phenotypes induced by the Ha-ras activation in the MCF7 cell-line.

The acquisition of a motile and invasive phenotype is an important step in the development of tumors and, ultimately, metastasis. This step requires the abrogation of cell–cell contacts, the remodelling (degradation, component changes) of the ECM and cell–matrix interactions, together with increased cell motility mediated by the actin cytoskeleton, accelerated cellular proliferation and escape from pro-apoptotic mechanisms, which cumulatively lead to a tumorigenic phenotype (5).

Our analysis reveals that Ha-ras activation in MCF7 appears to induce persistent remodelling of both cytoskeleton and discrete adhesive structures mediated by under-expression of the Arp2/3 complex, Hsp27 and profilin, together with thymosin β4 over-expression (6–10). This, in turn, could induce a decrease in the formation of Focal Adhesion (FA)

A
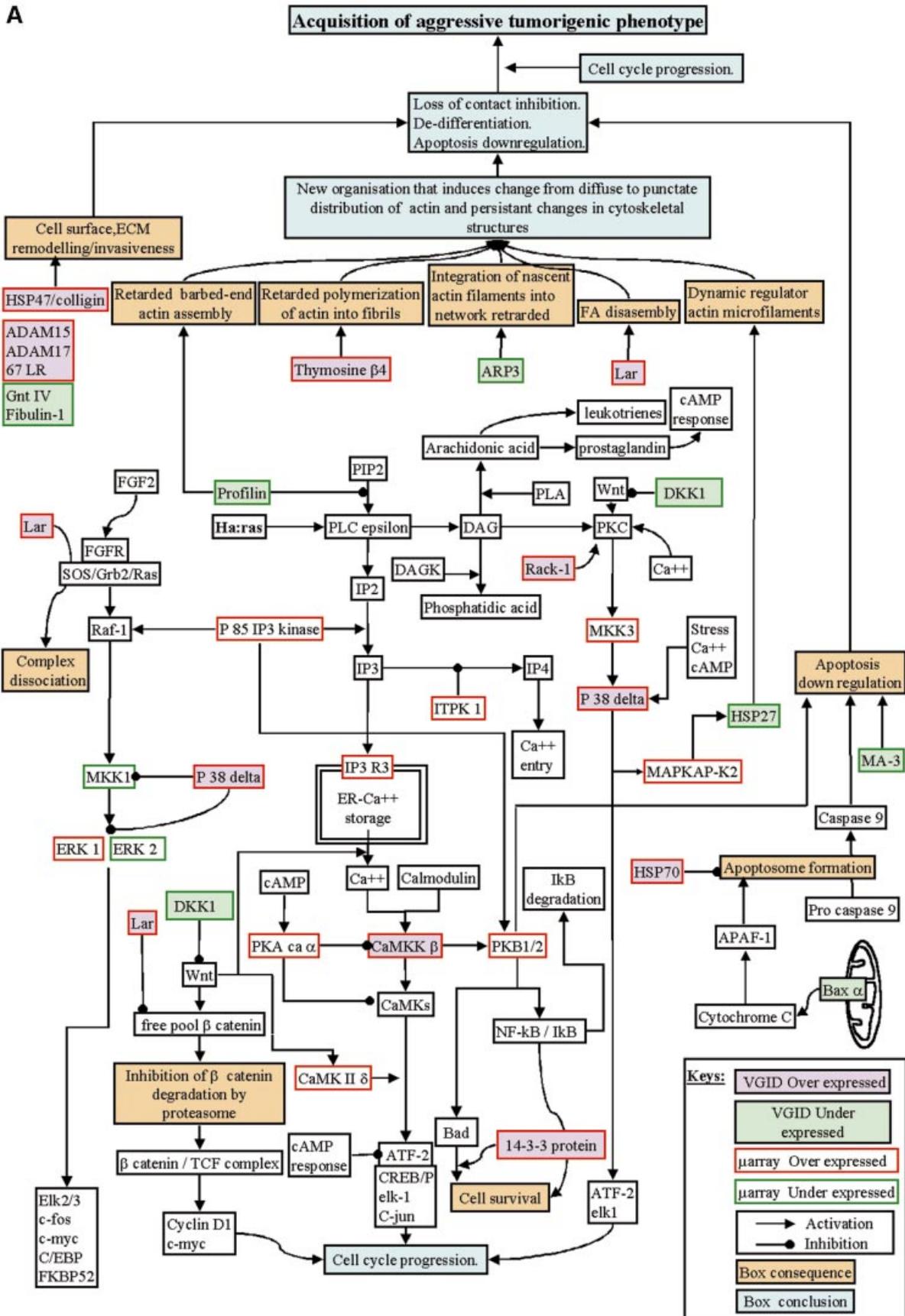
patches, the sites of cell–ECM and cell–cell interactions, leading to increases in cell motility, thus promoting invasiveness (Fig. 6A). In agreement with this postulate, the
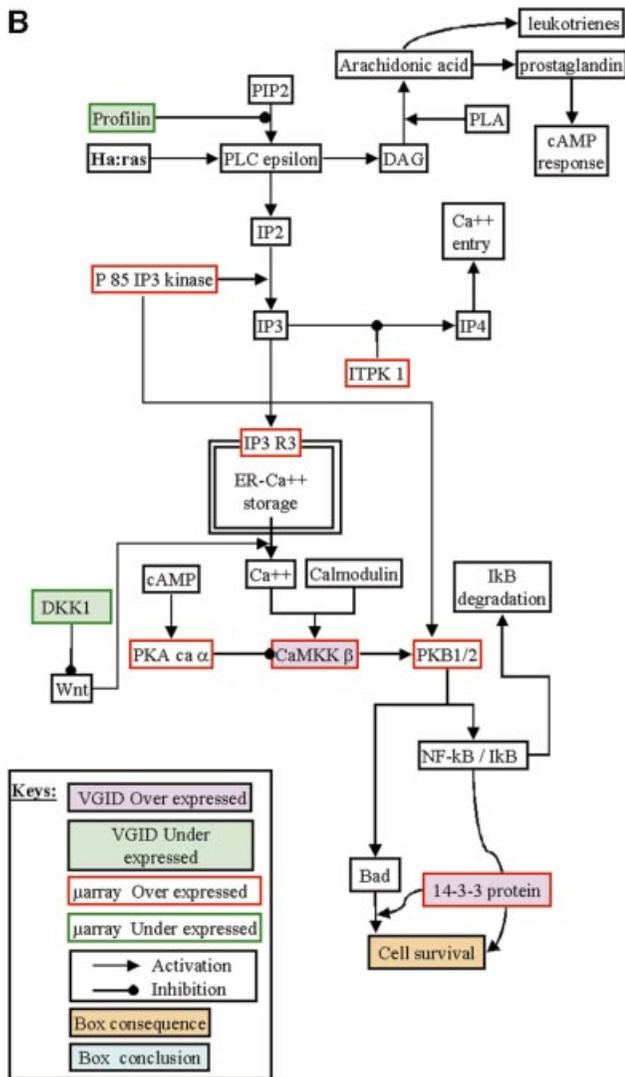

Figure 6. (**A**) Experimentally testable biological model derived from under- and over-expressed genes in MCF7-ras cells and published information. The gene expression data from VGID™ and microarray assays were integrated with extensive published information into a detailed and experimentally testable biological model. The diagram above depicts only the main cellular mechanisms suggested as the basis for Ha-ras dependent tumorigenic transformation of the MCF7 breast epithelial cell line. The 'consequence' and 'conclusion' boxes replace further detailed pathways which were taken into consideration to define theoretical points and modes of pharmacological interventions aiming to induce MCF7-ras-specific cell death. This graphic clearly shows that the Ca^{2+}-dependent and DAG/PIP3 signaling pathways (CaMKs, p38, etc.) together with the PKA/cAMP feedback pathways are centrally involved in the pathological process. Thus, Ha-ras activation seems to promote tumor progression through deregulation of these pathways. (**B**) Apoptosis-associated pathways affected by calcium. Calcium release from ER is known to be an important element in the PKB/NF-kappaB anti-apoptotic cascade through CamKKβ activation. Consequently, exacerbating the existing deregulation of calcium and its cAMP/PKA negative feedback, evidently present in the Ha-ras-associated tumor progression mechanism studied here, could specifically induce apoptotic cell death in MCF7-ras cells. This hypothesis was validated *in vitro* using two drugs known to maintain PKA activity while preventing the fall of intracellular cAMP levels and to increase calcium influx, respectively.

over-expression of LAR, a multifunctional protein tyrosine phosphatase (PTPase) which acts as receptor for cell surface and/or ECM molecules (11) and is known to be involved in FA disassembly (12), was detected in MCF7-ras (Table 1).
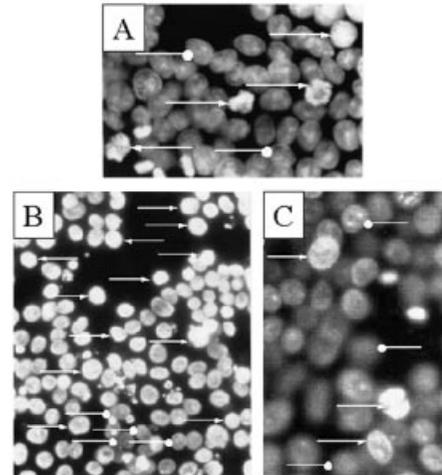
Modulations of ECM composition and organization appear crucial in breast neoplastic cell invasion and metastasis (13). Evidence of ECM remodeling in MCF7-ras was provided by seven genes (Fig. 6A). Two of these, the disintegrin metalloprotease ADAM17 and 15, are over-expressed more than 2-fold (Table 2). ADAM17 plays a key role in the maturation and cleavage of the membrane-anchored cytokine TNF-alpha, which induces the secretion of matrix metalloprotease 1 (MMP-1), a protease involved in the degradation of the ECM (14). ADAM15 appears to be involved in cell–cell or cell–matrix interactions and matrix degradation (15). Other proofs of ECM remodelling were provided by differential expression of Gnt-IV, Fibulin-1, LAR, 67LR and colligin/Hsp47, which are directly associated with cell–cell and cell–matrix attachment (Fig. 6A). Gnt-IV, found to be under-expressed, is one of the essential enzymes in the production of tri- and tetra-antennary Asn-linked sugar chains (16). Thus, variations in protein sugar antennary structures could induce cell surface modifications involved in cell–cell communication or adhesion. Fibulin-1, a secreted glycoprotein that becomes incorporated into fibrillar ECM and binds to fibronectin, inhibits cancer cell motility *in vitro*. Its under-expression plays a role in tumor formation and invasion in athymic mice (17). Over-expression of colligin/Hsp47 is associated with fibrosis (18), a phenomenon present in most breast cancers and apparently associated with the formation of aberrant collagen bundles which may, in turn, facilitate breast tumor invasion (19). 67LR is known to interact with laminin, the major glycoprotein of basement membranes. Over-expression of the 67LR is a consistent event appearing when cancer cells acquire an invasive and metastatic phenotype (20). Transfection of MCF7 cells with the Ha-ras oncogene has been shown to induce a greater ability of cells to migrate and attach to a laminin substrate, to grow in the presence of a basement membrane matrix and to cross the barrier of basement membranes (21). Thus, 67 LR over-expression could promote tumor cell adhesion to the basement membrane, thereby facilitating lamina digestion by ADAMs such as ADAM15 and 17, followed by wide dissemination in the body.

Concurrently, as shown in Figure 6A, Ha-ras constitutive activation in MCF7 cells gave down-regulation of pro-apoptotic mechanisms. Modulation of MA-3 mRNA expression is associated with apoptosis (22). Moreover, low expression of Bax-α, a pro-apoptotic ion channel forming protein involved in the release of mitochondrial cytochrome *c* that then leads to caspase activation, correlates with anti-apoptotic features (23). The inhibition of Hsp70 synthesis has been shown to induce massive death of human breast cancer cells, including MCF7, whereas the survival of non-tumorigenic breast epithelial cells is not affected (24). The release of cytochrome *c* from mitochondria by apoptotic signals induces the formation of the oligomeric Apaf-1-caspase-9 apoptosome. By direct binding to Apaf-1, Hsp70 acts as an inhibitor of apoptosome formation, thus preventing the recruitment of caspases to the complex (25). But to ensure cell survival, anti-apoptotic signaling arising from the inositol/Ca^{2+}/PKC/Wnt/PKA pathways should also be required. Thus the expression of
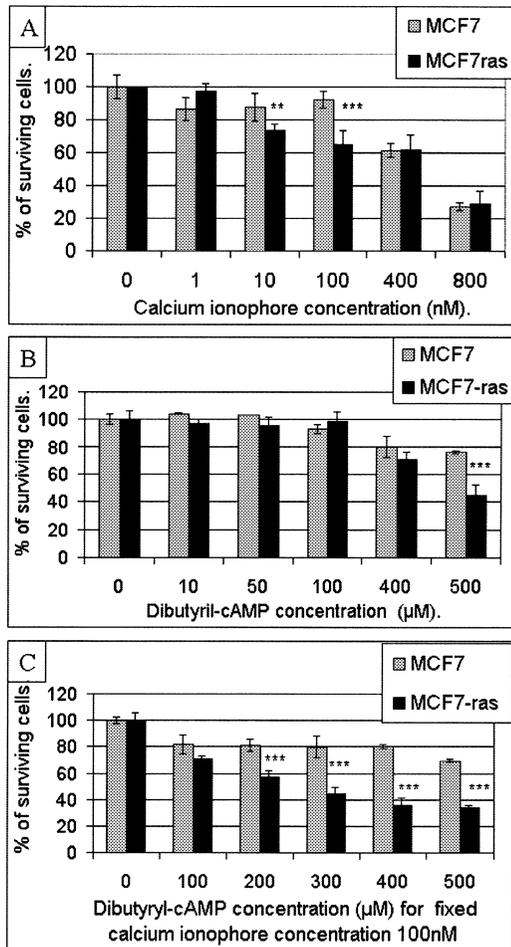
Figure 7. Testing the points and modes of intervention suggested by the model. A23187 and db-cAMP were used as specific drugs against the MCF7-ras cells. The results in (**A**) and (**B**) show that, used singly, A23187, at a concentration equal to 100 nM, and db-cAMP, at a concentration equal to 500 μM, induce moderate MCF7-ras-specific cell death, as compared to MCF7 cells. The results displayed in (**C**) show that MCF7-ras was uniquely sensitive to the association of the two drugs and the best differential response was obtained with a treatment consisting of 100 nM A23187 + 400 μM db-cAMP. These results confirmed that, in MCF7-ras cells, the pathways regulated by calcium mobilization and PKA/cAMP activation seem to play major roles in Ha-ras-dependent transformation. Statistical analyses were performed using the unpaired t-test with confidence intervals equal to 95%. Significant differences in response to treatment are indicated by ** and *** which correspond to P-values less than 0.005 and 0.001, respectively.

Figure 8. Apoptotic nuclei of MCF7 and MCF7-ras cells treated with A23187 + db-cAMP. The ionophore A23187 (100 nM) and db-cAMP (400 μM) were added to MCF7 (**A**) and MCF7-ras (**B**) cells for 48 h. Cell nuclei were stained with DAPI, as described in Materials and Methods, and the slides were observed under a fluorescence microscope. Apoptotic cells with chromatin condensation and DNA fragmentation, appearing as clear cells in the figures, are annotated with white arrows, indicating apoptotic mechanisms mainly present in treated MCF7-ras cells. Live cells, appearing as dark cells in the figures, are annotated with round-headed white arrows. For comparison, untreated MCF7-ras control cells are presented in (**C**).

oncogenic Ha-ras in rat intestinal epithelial cells results in the activation of PKB and the induction of anti-apoptotic signaling (26). Microarray gene expression analysis revealed that PKB 1/2 were up regulated in MCF7-ras (Table 2, Fig. 6A). Once activated by CaMKK (27) or via the IP3K pathway (28), PKB exerts anti-apoptotic effects through the phosphorylation of substrates such as caspase 9, NFkB kinases, and Bad, resulting in the sequestration of Bad by 14-3-3 proteins (27,29,30). Hence, in association with MA-3 and Bax-α repression together with Hsp70 and 14-3-3 ε over-expression, this mechanism is likely to provide protection against apoptosis in MCF7-ras.

Many genes identified by VGID™ as over-expressed such as p38δ kinase, CaMKKβ, Rack1, LAR, Diacyl glycerol kinase ζ (DAGKζ), Reticulocalbin, L-Plastin, TCP1θ, FKBP52, or under-expressed such as DKK1 and Profilin (Table 1) are involved in the inositol-PKC-PKA-Wnt signaling network which requires mobilization of internal Ca^{2+} stores (Fig. 6A). Profilin is known to bind phosphatidyl inositol 4-5 bisphosphate (PIP2) preventing its hydrolysis by unphosphorylated PLC (31) while DAGKζ terminates inositol signaling at the nuclear level. But this pathway is critically dependent upon the activity of regulatory genes such as ITPK1, p85 IP3K and IP3R3, all three of which were found to be over-expressed by microarray analysis, providing further evidence supporting up-regulation of inositol signaling in MCF7-ras (Fig. 6A). p85-IP3K phosphorylates inositol-2-phosphate (IP2) to inositol-3-phosphate (IP3), which, after binding to an IP3-receptor (32) such as IP3R3, induces Ca^{2+} release from the endoplasmic reticulum (ER). Concurrently, some IP3 is phosphorylated by ITPKI to form inositol 1,3,4,5-tetraphosphate (IP4). There is evidence suggesting that this may facilitate Ca^{2+} entry into the cell (33). In response to the increased intracellular Ca^{2+} level, CaMKKβ phosphorylates and activates CaMKs (27) which then regulate transcription through phosphorylation of several transcription factors, including cAMP-response element binding protein (CREB), activating transcription factor-2 (ATF-2), Elk-1 and C-jun (27,34). This cascade appears to be under the control of cAMP/PKA (27,35) and its inhibition by PKA is likely to modulate the balance between cAMP and Ca^{2+}-dependent signal transduction pathways (35), including the cross-talk between CaMKK and PKB associated with apoptosis regulation (27). PKAcaα, a key component of this regulatory loop,

Table 2. Specific microarray expression analyses

Genes	Accession number	Microarray ratio (cy5/cy3)	Status in MCF7-ras	VGID™ data set
MKK1	L05624	0.67 ± 0.10	–	No
MKK3	L36719	1.38 ± 0.01	+	No
Erk1	X60188	1.38 ± 0.07	+	No
Erk2	M84489	0.88 ± 0	–	No
PKB1	X61037	4.19 ± 0.29	+++	No
PKB2	M95936	2.04 ± 0.44	++	No
MAPKAPK-2	NM_004759	3.55 ± 1.32	+++	No
CaMKII beta	AF112472	1.03 ± 0.07		No
CaMKII delta	AF071569	1.69 ± 0	++	No
ITPKI	NM_014216	4.97 ± 0.73	+++	No
P85 IP3K	X80907	2.22 ± 0.36	++	No
IP3R3	NM_002224	2.52 ± 0.76	++	No
PKA ca alpha	NM_002730	1.83 ± 0.09	+	No
CaMKK beta	AF140507	1.54 ± 0.24	+	Yes
P38 delta	U93232	3.17 ± 0.24	+	Yes
DKK1	AF177394	0.12 ± 0.05	–	Yes
Profilin	J03191	0.63 ± 0	–	Yes
ADAM15	U46005	2.59 ± 0.19	++	Yes
ADAM17	XM_045348	2.04 ± 0.12	++	Yes
67LR	S37431	2.00 ± 0.15	+	Yes
HSP70	M11717	1.60 ± 0.14	+	Yes

In order to verify the validity of the initial integrative model, genes absent from the VGID™ data set, but playing key roles in the MCF7-ras-specific cellular alterations suggested by integrative analysis of the entire data set, were selected for microarray expression analyses. Some genes belonging to the VGID™ data set, the expression patterns and levels of which had already been ascertained, were included as controls. The corresponding amplicons, generated by PCR from MCF7 and MCF7-ras genomic DNA, were then used to construct microarrays on glass slides (Fig. 5). The data shown are the mean value of nine independent assays where each sequence was assayed in triplicate. Ratio values correspond to signal intensities of cyanine 5 fluorescence (MCF7-ras transcripts) over cyanine 3 fluorescence (MCF7 transcripts). A ratio superior to 1 indicates that the corresponding gene is over-expressed in MCF7-ras and a ratio inferior to 1 that the gene is under-expressed in MCF7-ras. (+) or (–) in the status column provide a rapid reading of the expression status in MCF7-ras. The last column indicates the genes isolated with the VGID™ technology.

was found to be over-expressed in MCF7-ras (Table 2), suggesting an increased cross-talk activity between inositol and Ca^{2+}-dependent pathways (Fig. 6A). Here, the kinase p38δ, the downstream effector of MKK3, which was found over-expressed, and MKK6, play a key role. PKC appears to be the first lead to the activation of p38δ mediated by MKK3 (36,37) (Table 2, Fig. 6A). PKC requires Rack-1 and Ca^{2+} for effective translocation to the cytoplasmic membrane and signaling activity, respectively, in response to diacylglycerol (DAG) (38). PKA, through the generation of reactive oxygen species, further activates p38 and its downstream effectors such as MAPKAPK-2 (Table 2) and the transcription factors ATF-2 and Elk-1 (37,39). p38-dependent MAPKAPK-2 is the best-characterized upstream effector of Hsp27 (40) which plays a significant role in actin filament dynamics and, therefore, affects the integrity of the cytoskeleton (6) (Fig. 6A).

Activation of ras is known to induce the MAPK/Erk kinase signaling pathway (41) but we found, by microarray gene expression analyses, that MKK1 and Erk2 were under-expressed in MCF7-ras cells (Fig. 6A, Table 2). Furthermore, our analysis strongly suggested that Ha-ras does not act through the canonical ras pathway but through an entirely different set of mechanisms. Constitutively activated GTP-Ha-ras binds to and translocates with PLCε from the cytosol to the plasma membrane and stimulates the PIP2-hydrolyzing activity of PLCε (42,43). Thus, PLCε appears to be the prime element in Ha-ras-dependent signaling, resulting in the constitutive activation of the phosphoinositol pathway which activates PKC through the production of DAG, and leads to the mobilization of Ca^{2+} storage via IP3.

The ensuing rise in cytoplasmic Ca^{2+} and PKC activation cumulatively leads to persistent cytoskeletal reorganization and activation of several transcription factors. Specific activation of p38δ results in a potent inhibition of the activity of Erk1/2 and its upstream activator MKK1/2 (44). Furthermore, LAR can inhibit receptor-induced Erk activation by preventing phosphorylation of both the 180 kDa protein and FRS2, two signal transducers that act downstream of growth-factor receptors (45) where FRS2 interacts with Grb2, which then binds to ras. Thus, up-regulation of p38δ and LAR may lead to competitive down-regulation of the Erk signaling pathway and this could explain why Erk2 signaling, induced by Ras/Rac-1 activation and expected to be active in cultured cells, is down-regulated in MCF7-ras.

The HMG box transcription factors of the lymphoid enhancing factor/T-cell factor (LEF/TCF) family associate with β-catenin and the resulting transcription factor complexes can subsequently regulate cell-cycle control elements such as c-myc and cyclin D1 (46,47). This requires the involvement of the Wnt signaling pathway and Wnt family members which induce β-catenin stabilization. DKK-1, the most potent known indirect repressor of β-catenin, has been shown to antagonize Wnt signaling (48). DKK-1 is down-regulated more than 8-fold in MCF7-ras (Table 2), thus indicating that the indirect up-regulation of the Wnt signaling pathway plays an important role in promoting transformation and cell growth in MCF7-ras via gene derepression and escape from cyclin D cell-cycle regulation (Fig. 6A). Wnt family members can also stimulate intracellular Ca^{2+} release and the activation of CaMK II and PKC (49). In this respect, we found

that CaMKII δ (but not CaMKII β) was over-expressed in MCF7-ras cells, indicating that the cross-talk between the Wnt and calcium-regulated pathways, via CaMKII δ, is activated in MCF7-ras cells (Fig. 6A). Here LAR, which appears to control β-catenin signaling functions in opposition to Wnt signaling, could also play a significant role. The LAR protein has been shown to interact with β-catenin in the cadherin/catenin complex, preventing its phosphorylation and subsequent degradation (50). Thus, LAR over-expression concurrently with DKK-1 repression could lead to the dominance of Wnt signaling over β-catenin (Fig. 6A).

In the presence of persistent cytoskeleton remodeling, this series of events is likely to induce further modifications of the membrane targeting mechanisms, resulting in increased membrane plasticity and modifications of signal transduction pathways, Golgi structures and vesicle trafficking. Together with the mechanisms described above, such as cytoskeletal remodeling, matrix integrity/composition, apoptosis deregulation, these may cumulatively promote tumor progression, invasiveness and metastasis associated with the constitutive activation of Ha-ras in MCF7 cells.

According to this model (Fig. 6A), the Ha-ras transformation process is induced and maintained through the up-regulation of the inositol + Ca^{2+} + PKC + Wnt pathways triggering the induction of PKA-mediated feedback mechanisms which maintain overall cellular homeostatic equilibrium. The model thus suggests that exacerbating at least one of the up-regulated pathways (here calcium-dependent kinases and PKB activities) while concurrently impeding feedback mechanisms (here cAMP/PKA signaling) should result in MCF7-ras-specific cell death (Fig. 6B). This hypothesis was directly tested *in vitro* by treatments of MCF7 and MCF7-ras cells using the ionophore A23187 and db-cAMP singly and in combination. Here, the utilization of db-cAMP fulfils two distinct purposes: to maintain PKA in an active state while preventing the utilization of intracellular cAMP. The aim here is not to inhibit the PKA-mediated feedback mechanisms, but to exacerbate the effects of moderate calcium influx which, through their effects upon the PKC pathways, should lead to increases in the levels of intracellular cAMP. Therefore, the cumulative effects of db-cAMP associated with calcium influx would be to further exacerbate the existing alterations in cytoskeletal and vesicle-transport dynamics, eventually resulting in the lethal disorganization of signaling pathways and intracellular transport mechanisms. Our results show that A23187 and db-cAMP alone induce moderate MCF7-ras-specific cell-death, corresponding to 25% and 31% with 100 nM A23187 and 500 μM db-cAMP, respectively, as compared to MCF7 cells. These results indicate that the signaling pathways which are affected by A23187 and db-cAMP correlate with Ha-ras constitutive activation and are potentially important in the associated tumor progression process. Furthermore, the combination of the two drugs clearly reveals that their simultaneous action on these signaling pathways significantly increases the rate of MCF7-ras-specific cell death. Thus, less than 40% of the MCF7-ras cells survived the combination of 100 nM A23187 and 400 μM db-cAMP treatment, as compared to a survival rate of at least 80% for MCF7 cells (Fig. 7C). These observations may also explain why the canonical ras-inducible

pathways cannot be correlated with the over-expression of P21 Ha-ras and tumor formation in nude mice (3).

We nevertheless also observed the presence of MCF7-ras cell populations resistant to the drug combination as well as that of sensitive MCF7 cell populations. Heterogeneity of populations has been demonstrated in MCF7 cell cultures (51) and our results could be explained by heterogeneity in subclonal populations. Since the treatment leading to cell death did not include cytotoxic compounds, cell death was likely to be largely due to apoptosis. This was confirmed by fluorescence microscopy observations on samples of treated cells, where chromatin condensation and DNA fragmentation, practically absent from the untreated cell samples, were observed in MCF7-ras cells as compared to MCF7 cells after DAPI nuclei staining (Fig. 8). The MCF7-ras-specific cell death, obtained after a 48 h exposure to the two drugs, clearly supported the model-derived hypothesis, thereby indicating that this integrative approach constitutes a valid means of deciphering complex biological processes in higher eukaryotic cells.

In the work presented here, activity modulations of the enzymes involved in the mechanisms uncovered and their regulations were not directly analyzed. In spite of this limitation, the integrative analytical methods reported here appear particularly powerful for generating directly testable biological models suggesting detailed interactive networks functionally associated with complex biological phenomena. A global understanding of internal cellular mechanism alterations is extremely important in predicting complex cellular behaviour and suggesting new hypotheses for the determination of therapeutic targets and modes of therapeutic intervention. We expect that, as the maturation of proteomics technologies proceeds, there will be a significant increase in the availability of pertinent and unambiguous protein data. Integrative approaches, such as that described here, will then gain in accuracy and breadth of utilization.

REFERENCES

1. Ozer,E., Sis,B., Ozen,E., Sakizli,M., Canda,T. and Sarioglu,S. (2000) BRCA1, C-erbB-2 and H-ras gene expressions in young women with breast cancer. An immunohistochemical study. *Appl. Immunohistochem. Mol. Morphol.*, **8**, 12–18.
2. Kasid,A., Lippman,M.E., Papageorge,A.G., Lowy,D.R. and Gelmann,E.P. (1985) Transfection of v-rasH DNA into MCF-7 human breast cancer cells bypasses dependence on estrogen for tumorigenicity. *Science*, **228**, 725–728.
3. Sommers,C.L., Papageorge,A., Wilding,G. and Gelmann,E.P. (1990) Growth properties and tumorigenesis of MCF-7 cells transfected with isogenic mutants of rasH. *Cancer Res.*, **50**, 67–71.
4. Ermolaeva,O., Rastogi,M., Pruitt,K.D., Schuler,G.D., Bittner,M.L., Chen,Y., Simon,R., Meltzer,P., Trent,J.M. and Boguski,M.S. (1998) Data management and analysis for gene expression arrays. *Nature Genet.*, **20**, 19–23.

5a. Yang,G.P., Ross,D.T., Kuang,W.W., Brown,P.O. and Weigel,R.J. (1999) Combining SSH and cDNA microarrays for rapid identification of differentially expressed genes. *Nucleic Acids Res.*, **27**, 1517–1523.

5. Nicolson,G.L. and Moustafa,A.S. (1998) Metastasis-associated genes and metastatic tumor progression. *In Vivo*, **12**, 579–588.

6. Mairesse,N., Horman,S., Mosselmans,R. and Galand,P. (1996) Antisense inhibition of the 27 kDa heat shock protein production affects growth rate and cytoskeletal organization in MCF-7 cells. *Cell Biol. Int.*, **20**, 205–212.

7. Cooper,J.A. and Schafer,D.A. (2000) Control of actin assembly and disassembly at filament ends. *Curr. Opin. Cell Biol.*, **12**, 97–103.

8. Svitkina,T.M. and Borisy,G.G. (1999) Arp2/3 complex and actin depolymerizing factor/cofilin in dendritic organization and treadmilling of actin filament array in lamellipodia. *J. Cell Biol.*, **145**, 1009–1026.

9. Kang,F., Purich,D.L. and Southwick,F.S. (1999) Profilin promotes barbed-end actin filament assembly without lowering the critical concentration. *J. Biol. Chem.*, **274**, 36963–36972.

10. Safer,D., Sosnick,T.R. and Elzinga,M. (1997) Thymosin beta 4 binds actin in an extended conformation and contacts both the barbed and pointed ends. *Biochemistry*, **36**, 5806–5816.

11. Brady-Kalnay,S.M. and Tonks,N.K. (1995) Protein tyrosine phosphatases as adhesion receptors. *Curr. Opin. Cell Biol.*, **7**, 650–657.

12. Serra-Pages,C., Kedersha,N.L., Fazikas,L., Medley,Q., Debant,A. and Streuli,M. (1995) The LAR transmembrane protein tyrosine phosphatase and a coiled-coil LAR-interacting protein co-localize at focal adhesions. *EMBO J.*, **14**, 2827–2838.

13. Hagedorn,H.G., Bachmeier,B.E. and Nerlich,A.G. (2001) Synthesis and degradation of basement membranes and extracellular matrix and their regulation by TGF-beta in invasive carcinomas (Review). *Int. J. Oncol.*, **18**, 669–681.

14. Gottschalk,C., Malberg,K., Arndt,M., Schmitt,J., Roessner,A., Schultze,D., Kleinstein,J. and Ansorge,S. (2000) Matrix metalloproteinases and TACE play a role in the pathogenesis of endometriosis. *Adv. Exp. Med. Biol.*, **477**, 483–486.

15. Kratzschmar,J., Lum,L. and Blobel,C.P. (1996) Metargidin, a membrane-anchored metalloprotease-disintegrin protein with an RGD integrin binding sequence. *J. Biol. Chem.*, **271**, 4593–4596.

16. Fukuta,K., Abe,R., Yokomatsu,T., Kono,N., Asanagi,M., Omae,F., Minowa,M.T., Takeuchi,M. and Makino,T. (2000) Remodeling of sugar chain structures of human interferon-gamma. *Glycobiology*, **10**, 421–430.

17. Qing,J., Maher,V.M., Tran,H., Argraves,W.S., Dunstan,R.W. and McCormick,J.J. (1997) Suppression of anchorage-independent growth and matrigel invasion and delayed tumor formation by elevated expression of fibulin-1D in human fibrosarcoma-derived cell lines. *Oncogene*, **15**, 2159–2168.

18. Razzaque,M.S. and Taguchi,T. (1999) The possible role of colligin/HSP47, a collagen-binding protein, in the pathogenesis of human and experimental fibrotic diseases. *Histol. Histopathol.*, **14**, 1199–1212.

19. Kauppila,S., Stenback,F., Risteli,J., Jukkola,A. and Risteli,L. (1998) Aberrant type I and type III collagen gene expression in human breast cancer *in vivo*. *J. Pathol.*, **186**, 262–268.

20. Stallmach,A., Orzechowski,H.D., Feldmann,P., Riecken,E.O., Zeitz,M. and Herbst,H. (1999) 32/67-kD laminin receptor expression in human colonic neoplasia: elevated transcript levels correlate with the degree of epithelial dysplasia. *Am. J. Gastroenterol.*, **94**, 3341–3347.

21. Albini,A., Graf,J., Kitten,G.T., Kleinman,H.K., Martin,G.R., Veillette,A. and Lippman,M.E. (1986) 17 beta-estradiol regulates and v-Ha-ras transfection constitutively enhances MCF7 breast cancer cell interactions with basement membrane. *Proc. Natl Acad. Sci. USA*, **83**, 8182–8186.

22. Shibahara,K., Asano,M., Ishida,Y., Aoki,T., Koike,T. and Honjo,T. (1995) Isolation of a novel mouse gene MA-3 that is induced upon programmed cell death. *Gene*, **166**, 297–301.

23. Bargou,R.C., Wagener,C., Bommert,K., Mapara,M.Y., Daniel,P.T., Arnold,W., Dietel,M., Guski,H., Feller,A., Royer,H.D. and Dorken,B. (1996) Overexpression of the death-promoting gene bax-alpha which is downregulated in breast cancer restores sensitivity to different apoptotic stimuli and reduces tumor growth in SCID mice. *J. Clin. Invest.*, **97**, 2651–2659.

24. Nylandsted,J., Rohde,M., Brand,K., Bastholm,L., Elling,F. and Jaattela,M. (2000) Selective depletion of heat shock protein 70 (Hsp70) activates a tumor-specific death program that is independent of caspases and bypasses Bcl-2. *Proc. Natl Acad. Sci. USA*, **97**, 7871–7876.

25. Saleh,A., Srinivasula,S.M., Balkir,L., Robbins,P.D. and Alnemri,E.S. (2000) Negative regulation of the Apaf-1 apoptosome by Hsp70. *Nat. Cell Biol.*, **2**, 476–483.

26. Sheng,H., Shao,J. and DuBois,R.N. (2001) Akt/PKB activity is required for Ha-Ras-mediated transformation of intestinal epithelial cells. *J. Biol. Chem.*, **276**, 14498–14504.

27. Soderling,T.R. (1999) The Ca-calmodulin-dependent protein kinase cascade. *Trends Biochem. Sci.*, **24**, 232–236.

28. Burgering,B.M. and Coffer,P.J. (1995) Protein kinase B (c-Akt) in phosphatidylinositol-3-OH kinase signal transduction. *Nature*, **376**, 599–602.

29. Cardone,M.H., Roy,N., Stennicke,H.R., Salvesen,G.S., Franke,T.F., Stanbridge,E., Frisch,S. and Reed,J.C. (1998) Regulation of cell death protease caspase-9 by phosphorylation. *Science*, **282**, 1318–1321.

30. Romashkova,J.A. and Makarov,S.S. (1999) NF-kappaB is a target of AKT in anti-apoptotic PDGF signalling. *Nature*, **401**, 86–90.

31. Lu,P.J., Shieh,W.R., Rhee,S.G., Yin,H.L. and Chen,C.S. (1996) Lipid products of phosphoinositide 3-kinase bind human profilin with high affinity. *Biochemistry*, **35**, 14027–14034.

32. Berridge,M.J. (1993) Inositol trisphosphate and calcium signalling. *Nature*, **361**, 315–325.

33. Luckhoff,A. and Clapham,D.E. (1992) Inositol 1,3,4,5-tetrakisphosphate activates an endothelial Ca(2+)-permeable channel. *Nature*, **355**, 356–358.

34. Ban,N., Yamada,Y., Someya,Y., Ihara,Y., Adachi,T., Kubota,A., Watanabe,R., Kuroe,A., Inada,A., Miyawaki,K., Sunaga,Y., Shen,Z.P., Iwakura,T., Tsukiyama,K., Toyokuni,S., Tsuda,K. and Seino,Y. (2000) Activating transcription factor-2 is a positive regulator in CaM kinase IV-induced human insulin gene expression. *Diabetes*, **49**, 1142–1148.

35. Matsushita,M. and Nairn,A.C. (1999) Inhibition of the Ca2+/calmodulin-dependent protein kinase I cascade by cAMP-dependent protein kinase. *J. Biol. Chem.*, **274**, 10086–10093.

36. Keesler,G.A., Bray,J., Hunt,J., Johnson,D.A., Gleason,T., Yao,Z., Wang,S.W., Parker,C., Yamane,H., Cole,C. and Lichenstein,H.S. (1998) Purification and activation of recombinant p38 isoforms alpha, beta, gamma and delta. *Protein Expr. Purif.*, **14**, 221–228.

37. Raingeaud,J., Whitmarsh,A.J., Barrett,T., Derijard,B. and Davis,R.J. (1996) MKK3- and MKK6-regulated gene expression is mediated by the p38 mitogen-activated protein kinase signal transduction pathway. *Mol. Cell. Biol.*, **16**, 1247–1255.

38. Mochly-Rosen,D., Khaner,H. and Lopez,J. (1991) Identification of intracellular receptor proteins for activated protein kinase C. *Proc. Natl Acad. Sci. USA*, **88**, 3997–4000.

39. Pomerance,M., Abdullah,H.B., Kamerji,S., Correze,C. and Blondeau,J.P. (2000) Thyroid-stimulating hormone and cyclic AMP activate p38 mitogen-activated protein kinase cascade. Involvement of protein kinase A, rac1 and reactive oxygen species. *J. Biol. Chem.*, **275**, 40539–40546.

40. Cohen,M.V., Baines,C.P. and Downey,J.M. (2000) Ischemic preconditioning: from adenosine receptor of KATP channel. *Annu. Rev. Physiol.*, **62**, 79–109.

41. Salh,B., Marotta,A., Matthewson,C., Ahluwalia,M., Flint,J., Owen,D. and Pelech,S. (1999) Investigation of the Mek-MAP kinase-Rsk pathway in human breast cancer. *Anticancer Res.*, **19**, 731–740.

42. Song,C., Hu,C.D., Masago,M., Kariyai,K., Yamawaki-Kataoka,Y., Shibatohge,M., Wu,D., Satoh,T. and Kataoka,T. (2001) Regulation of a novel human phospholipase C, PLCepsilon, through membrane targeting by Ras. *J. Biol. Chem.*, **276**, 2752–2757.

43. Kelley,G.G., Reks,S.E., Ondrako,J.M. and Smrcka,A.V. (2001) Phospholipase C (epsilon): a novel Ras effector. *EMBO J.*, **20**, 743–754.

44. Westermarck,J., Li,S.P., Kallunki,T., Han,J. and Kahari,V.M. (2001) p38 mitogen-activated protein kinase-dependent activation of protein phosphatases 1 and 2A inhibits MEK1 and MEK2 activity and collagenase 1 (MMP-1) gene expression. *Mol. Cell. Biol.*, **21**, 2373–2383.

45. Wang,X., Weng,L.P. and Yu,Q. (2000) Specific inhibition of FGF-induced MAPK activation by the receptor-like protein tyrosine phosphatase LAR. *Oncogene*, **19**, 2346–2353.

46. He,T.C., Sparks,A.B., Rago,C., Hermeking,H., Zawel,L., da Costa,L.T., Morin,P.J., Vogelstein,B. and Kinzler,K.W. (1998) Identification of c-MYC as a target of the APC pathway. *Science*, **281**, 1509–1512.

47. Shtutman,M., Zhurinsky,J., Simcha,I., Albanese,C., D'Amico,M., Pestell,R. and Ben-Ze'ev,A. (1999) The cyclin D1 gene is a target of the beta-catenin/LEF-1 pathway. *Proc. Natl Acad. Sci. USA*, **96**, 5522–5527.

48. Fedi,P., Bafico,A., Nieto Soria,A., Burgess,W.H., Miki,T., Bottaro,D.P., Kraus,M.H. and Aaronson,S.A. (1999) Isolation and biochemical characterization of the human Dkk-1 homologue, a novel inhibitor of mammalian Wnt signalling. *J. Biol. Chem.*, **274**, 19465–19472.

49. Kuhl,M., Sheldahl,L.C., Park,M., Miller,J.R. and Moon,R.T. (2000) The Wnt/Ca2+ pathway: a new vertebrate Wnt signalling pathway takes shape. *Trends Genet.*, **16**, 279–283.

50. Muller,T., Choidas,A., Reichmann,E. and Ullrich,A. (1999) Phosphorylation and free pool of beta-catenin are regulated by tyrosine kinases and tyrosine phosphatases during epithelial cell migration. *J. Biol. Chem.*, **274**, 10173–10183.

51. Devarajan,E., Chen,J., Multani,A.S., Pathak,S., Sahin,A.A. and Mehta,K. (2002) Human breast cancer MCF-7 cell line contains inherently drug-resistant subclones with distinct genotypic and phenotypic features. *Int. J. Oncol.*, **20**, 913–920.